Probabilistic failure analysis of stochastically excited nonlinear structural systems with fractional derivative elements

Marco Behrendt[1*], Vasileios C. Fragkoulis[2], George D. Pasparakis[3], Michael Beer[4,2,5]

[1] *Department of Civil and Environmental Engineering, Rice University, 6100 Main Street, Houston, TX 77005, USA*

[2] *Department of Civil and Environmental Engineering, University of Liverpool, Liverpool, L69 3GH, UK*

[3] *Department of Civil and Systems Engineering, Johns Hopkins University, 3400 N. Charles Street, Baltimore, MD 21218, USA*

[4] *Institute for Risk and Reliability, Leibniz Universität Hannover, Callinstraße 34, 30167 Hannover, Germany*

[5] *International Joint Research Center for Resilient Infrastructure & International Joint Research Center for Engineering Reliability and Stochastic Mechanics, Tongji University, 1239 Siping Road, Shanghai 200092, China*

Abstract

In this paper, the application of the relaxed power spectral density (PSD) framework is developed for quantifying uncertainties in dynamical systems with fractional derivative elements. The proposed methodology offers a systematic treatment of uncertainties in spectrum-based stochastic simulation and their propagation for response determination of systems with memory-dependent or viscoelastic behavior. A key advantage of the framework lies in its ability to model the variability of estimated PSD functions using a non-parametric probabilistic representation, while explicitly accounting for frequency-domain correlations that are typically overlooked in conventional PSD-based estimates. First, a "relaxed" version of the power spectral density is derived by extracting statistical moments across ensembles of discretized PSD estimates. Next, frequency-dependent truncated normal distributions are employed to capture PSD uncertainties. Statistically compatible realizations are generated using three distinct sampling strategies: a single-variable inverse cumulative distribution function-based method for efficient sampling of marginal probability

*marco.behrendt@rice.edu

density functions, a multivariate Gaussian approach that incorporates cross-frequency covariance to capture global correlation structure, and an Ornstein–Uhlenbeck Markov process model, which reconstructs smoothly correlated PSD trajectories. The efficiency of the proposed approach is demonstrated by considering three representative case studies. These are a Duffing nonlinear oscillator with fractional damping, a tuned mass-damper-inerter system with nonlinear coupling characteristics, and a nonlinear vibration energy harvester under stochastic excitation. It is shown that by accounting for a comprehensive probabilistic treatment of the PSD, the proposed framework yields enhanced reliability analysis results of dynamical systems under spectral uncertainty.

Keywords: Stochastic dynamics, Fractional derivatives, Power spectral density function, Uncertainty quantification, Structural reliability analysis.

1 Introduction

Efficiently assessing the reliability of structural systems subjected to dynamic loads is critical for ensuring the safety, stability, and functionality of structures across various engineering disciplines. These dynamic loads can originate from natural phenomena, such as earthquakes, wind, and waves, as well as from human activities, including traffic, machinery, and construction operations. They often exhibit random characteristics and are therefore effectively modeled as stochastic processes [1, 2]. Unlike deterministic cases, stochastic loads induce complex responses that depend on the properties of the system in question, complicating the analysis of its response and necessitating the adoption of appropriate probabilistic approaches [3, 4]. Nevertheless, this analysis is essential for ensuring the reliability and resilience of structures, especially in critical infrastructure where uncertainty could lead to catastrophic failures.

Assessing the reliability of structural systems can also be challenging due to the inclusion of fractional order terms in the equations governing the system dynamics, not to mention the stochastic nature of the applied loads and the nonlinearities that are typical in most systems. In recent years, fractional calculus has increasingly been applied in engineering, spanning innovative non-local continuum models (e.g., [5]) to vibration energy harvesting (e.g., [6, 7]). It has been widely employed in structural engineering

to model the viscoelastic behavior of materials (e.g., [8]), with the modeling of viscoelastic dampers being one of the most relevant applications in seismic isolation (e.g., [9, 10]). More recent applications in earthquake engineering pertain to the response analysis and reliability assessment of systems that conform to modern seismic design codes (e.g., [11, 12, 13]). Additionally, various methodologies have been proposed within the field of stochastic dynamics to assess the stochastic response and reliability of systems with fractional derivatives. These methods encompass techniques based on statistical linearization (e.g., [14, 15, 16, 17]), memory-free formulation methods (e.g., [18, 19]), strategies utilizing the globally evolving generalized density evolution equation (e.g., [20]), frameworks that employ Wiener path integrals (e.g., [21]), even approaches to address the challenging case of systems with singular parameter matrices and constraints (e.g., [22, 23, 24]).

Failure probability estimation constitutes a persistent challenge in stochastic dynamics and is a fundamental aspect of structural reliability analysis [25, 26, 27]. These estimates are used to quantify the performance of structures subjected to random vibrations under specified conditions, thereby ensuring their safety and durability. To this end, several approaches have been proposed to efficiently assess the failure probabilities of structural systems, with the ultimate goal of minimizing failure risks and enhancing their resilience, even in uncertain and dynamically varying conditions. These approaches range from semi-analytical methods (e.g., [28]) to purely numerical Monte Carlo simulation (MCS) schemes (e.g., [29]), including, among others, reliability index methods (e.g., [30]), stochastic finite element-based techniques (e.g., [31]), Bayesian methods (e.g., [32]), probabilistic sensitivity analysis frameworks (e.g., [33]), and frameworks based on stochastic averaging (e.g., [34]). More recently, advanced sampling strategies such as Bayesian active learning and line sampling have been developed to improve efficiency in estimating rare-event probabilities (e.g., [35, 36]).

Spectral analysis serves as a valuable tool for assessing the dynamic response of structures, as it provides the frequency content of dynamic loads and thus a clearer picture of how random excitations impact the system's behavior. Analyzing the power spectral density (PSD) function of dynamic loads and structural responses facilitates the identification of resonant frequencies, the development of damping strategies and performance-based structural optimization [37, 38]. However, the effectiveness of spectral analysis is often challenged by uncertainties associated with data acquisition and estimation of the underlying spectra. To address this, modern efforts have de-

veloped enhanced spectral modeling techniques. For instance, energy-based reckoning has been introduced to estimate evolutionary power spectra in non-stationary processes [39], and dimension-reduction spectral representations have enabled efficient reliability analysis in geotechnical systems [40]. A comprehensive review and reformulation of the spectral representation method (SRM) has also been presented in [41], offering a unifying framework for stochastic simulation in reliability applications.

Uncertainty quantification in the PSD function itself has emerged as a robust method for incorporating epistemic and aleatory uncertainty into dynamic reliability analysis. For instance, interval-based models, such as those presented in [42], address the imprecision in seismic power spectra by employing sets of recorded accelerograms, thereby accounting for the inherent variability in seismic inputs. Models that incorporate fractional derivatives, as discussed in [9, 10], enhance the reliability analysis of structures equipped with external viscoelastic dampers by considering parameter intervals and sensitivity under uncertain conditions. The probabilistic framework introduced in [43, 44] captures uncertainties arising from multiple data records by employing subjective probabilities to represent data-driven variability. This framework has been further extended in [45] to incorporate dependent frequency modeling and sampling, thereby enhancing the accuracy of failure probability estimation under complex dynamic interactions. These developments enable a more realistic representation of input uncertainty and improve failure probability estimation for complex systems such as those investigated in Ref. [46].

The present work focuses on integrating the relaxed PSD concept, including correlated models, into the reliability analysis of nonlinear dynamical systems featuring fractional derivative elements. Recent advances in multivariate Gaussian field modeling, particularly those addressing nonlinear probabilistic dependencies and heterogeneous spatial variabilities [47], further support the importance of capturing correlation structures in reliability-driven simulations. Incorporating fractional calculus into engineering models is particularly valuable, as it enables an efficient and accurate representation of complex material and system behavior under stochastic excitation. To this end, a probabilistic framework is developed to estimate failure probabilities by modeling uncertainties in the excitation through a dataset of PSD functions. Unlike the standard relaxed PSD model, which assumes independence across frequency components, the proposed approach explicitly accounts for frequency correlations during PSD sampling. This leads to the generation

of more realistic PSD realizations that better reflect observed spectral characteristics, thereby improving the accuracy of downstream reliability assessments. The PSD model is embedded within a MCS framework, allowing uncertainties in the excitation to be propagated through systems with nonlinear and fractional-order dynamics. To demonstrate the capabilities of the proposed method, three nonlinear dynamical systems with fractional derivative elements are considered: a Duffing oscillator, a tuned mass-damper-inerter (TMDI) system, and a nonlinear vibration energy harvester. Each system is subjected to stochastic excitations characterized by different PSD forms, enabling a comparative evaluation of sampling strategies and their effect on failure probability estimates. Overall, the proposed framework advances probabilistic modeling techniques by linking spectral uncertainty to structural reliability in a physically consistent and computationally efficient manner.

The remainder of the paper is structured as follows. Section 2 introduces some basic concepts concerning PSD estimation and fractional derivatives-based modeling of multi-degree-of-freedom (MDOF) systems. In Section 3 the concept of the relaxed PSD including different sampling procedures is described. The application of the proposed framework is described in Section 4, while the numerical examples are presented in Section 5. The work is briefly summarized in the concluding remarks in Section 6.

2 Theoretical description

In this section, a concise discussion on the theoretical background and critical aspects of the current paper is presented. In this context, concepts pertaining to PSD estimation and generation of PSD compatible stochastic process realizations are discussed, and the equations governing the dynamics of MDOF systems comprising fractional derivative elements are defined.

2.1 Power spectral density estimation

The estimation of the stationary PSD is based on the discrete Fourier transform (DFT), which facilitates the analysis of the frequency content of discrete signals. PSD estimation is essential for the decomposition of a signal into its harmonic components and allows the identification and quantification of the contribution of each frequency component to the overall signal power. The

theoretical foundation for PSD estimation is based on the Wiener-Khinchin theorem, which establishes a mathematical relationship between the autocorrelation function $R_x(\tau)$ and the PSD function $S_x(\omega)$ of the signal $\mathbf{x}(t)$, where τ describes the time lag and ω is the frequency [26]. For a continuous-time, wide-sense stationary signal with infinite duration, this relationship is expressed by the pair

$$S_x(\omega) = \int_{-\infty}^{\infty} R_x(\tau) e^{-\mathrm{i}\omega\tau} d\tau \tag{1}$$

and

$$R_x(\tau) = \frac{1}{2\pi} \int_{-\infty}^{\infty} S_x(\omega) e^{\mathrm{i}\omega\tau} d\omega, \tag{2}$$

with i denoting the imaginary unit. However, in practical scenarios, signals are neither continuous nor of infinite length. Consequently, direct application of the Wiener-Khinchin theorem is not feasible, and alternative estimation methods must be employed.

A commonly used approach for PSD estimation is based on the periodogram [48]. The periodogram provides an approximation of the actual PSD by using the squared absolute value of the DFT of a finite length signal $\mathbf{x}(t) = \begin{bmatrix} x_0 & x_1 & \dots & x_{N_t-1} \end{bmatrix}^{\mathrm{T}}$. The estimator is defined as

$$\hat{S}_x(\omega_k) = \lim_{T\to\infty} \frac{(\Delta t)^2}{T} \left| \sum_{n=0}^{N_t-1} x_n e^{-2\pi \mathrm{i} k n / N_t} \right|^2, \tag{3}$$

where Δt is the time increment, T is the length of the signal, N_t is the total number of data points in $\mathbf{x}(t)$, and ω_k corresponds to the discrete angular frequencies. Although the periodogram provides a straightforward and intuitive method for spectral estimation, it suffers from limitations such as spectral leakage and high variance. Therefore, the periodogram estimates of power at any frequency can vary significantly from one realization to another, even for signals with the same underlying PSD. This turns the periodogram to a noisy and unstable estimator, especially for short datasets. To mitigate these issues, alternative methods were developed, such as the Bartlett's method [49, 50] or Welch's method [51], which both define well-known estimators. Bartlett's method involves dividing the time series data into non-overlapping segments, computing the periodogram for each segment, and then averaging these periodograms to reduce variance in the spectral estimate. This approach improves the stability of the estimate at the loss

of the frequency resolution. On the other hand, Welch's method extends Bartlett's method by allowing overlapping segments by applying a window function to each segment before the periodogram is calculated. The latter further reduces variance and spectral leakage, resulting in a smoother and more reliable spectral estimate.

Due to its advantages over Bartlett's approach, Welch's method is adopted herein. It is described briefly in the following. First, the time signal $\mathbf{x}(t)$ is divided into K segments, $\mathbf{x}_1(t) = \mathbf{x}(t^*)$, $\mathbf{x}_2(t) = \mathbf{x}(t^* + D)$, ..., $\mathbf{x}_K(t) = \mathbf{x}(t^* + (K-1)D)$, where $t^* = 0, 1, \ldots, L-1$ denotes the local time within the segment, L is the segment's length, and D accounts for the spacing between the segment start points. The parameter D controls the overlap degree, with $D = L/2$ resulting in 50% overlap, for instance. Then, each segment is windowed using a function $W(t^*)$. Various window functions can be applied to reduce spectral leakage. In this work, the Hamming window [52] is employed, which is defined as

$$W(t^*) = 0.54 - 0.46 \cos\left(\frac{2\pi t^*}{N_{t^*} - 1}\right), \quad 0 \leq t^* \leq N_{t^*} - 1. \tag{4}$$

The modified periodogram for each windowed segment is then computed as

$$P_k(\omega_m) = \frac{1}{L}\left|\sum_{t^*=0}^{L-1} \mathbf{x}_k(t^*) W(t^*) e^{-2\pi \mathrm{i} m t^*/L}\right|^2, \tag{5}$$

where $k = 1, 2, \ldots, K$, and ω_m corresponds to the frequency bins. The final PSD estimate is obtained by averaging the modified periodograms as

$$\hat{S}_x^W(\omega_m) = \frac{1}{K}\sum_{k=1}^{K} P_k(\omega_m). \tag{6}$$

2.2 The fractional derivative operator

Fractional calculus broadens the conventional concepts of differentiation and integration to include non-integer orders [53]. As an extension of classical calculus, it enables the calculation of derivatives and integrals of non-integer order, offering in this way a more adaptable framework for modeling complex systems and phenomena across various disciplines, including physics, finance, biology and engineering [54, 55, 56]. In terms of engineering applications, the

increasing use of fractional calculus is motivated by its proven ability to accurately and efficiently model the behavior of viscoelastic materials. Fractional order models are particularly well-suited to capture memory and hereditary effects, providing a more accurate representation of the material's constitutive behavior [57]. This, in turn, leads to a more precise determination of the system response compared to the corresponding classical integer-order models, especially in applications related to viscoelastic dampers utilized in vibration isolation and seismic isolation of engineering systems (e.g., [58]). Moreover, fractional order models allow for a continuous spectrum of relaxation times, rather than being limited to discrete values, and offer a compact formulation that reduces the complexity and number of parameters required for system modeling (e.g., [8]). These advantages are especially valuable when addressing uncertain or highly dynamic environments. The interested reader is directed to Ref. [57] for a detailed discussion on the topic.

Among the different definitions of fractional order derivatives, these of the Riemann-Liouville, the Caputo and the Grünwald-Letnikov fractional derivatives stand out as the most used ones in engineering applications [59, 60, 54]. Following the Riemann-Liouville definition, the fractional derivative of order q, $m-1 < q < m$ ($m \in \mathbb{N}$), of a continuous function $f(t)$ is given by

$$ {}_{RL}D^{q}_{a,t} f(t) = \frac{1}{\Gamma(n-q)} \frac{d^m}{dt^m} \int_a^t f(\tau)(t-\tau)^{-q+m-1} d\tau, \tag{7} $$

where $\Gamma(\cdot)$ denotes the gamma function. Although the Riemann-Liouville definition is widely used, it does not handle the initial conditions imposed in the problem under consideration in a straightforward manner, which can be burdensome in terms of applications.

To compensate for the latter, the Caputo definition of fractional order q is used ($m-1 < q < m$, $m \in \mathbb{N}$), which is given by

$$ {}_{C}D^{q}_{a,t} f(t) = \frac{1}{\Gamma(n-q)} \int_a^t f^{(m)}(\tau)(t-\tau)^{-q+m-1} d\tau. \tag{8} $$

A key difference between adopting the definitions given by Eqs. (7) and (8) is that the latter allows the initial conditions of the problem to be specified in terms of the function rather than its derivatives. Thus, the aspect that makes the Caputo definition compelling for engineering and physical problems is its treatment of initial conditions, which are typically expressed in terms of the function $f(t)$ [57, 60, 61].

Lastly, the Grünwald-Letnikov definition is based on a discrete approach and is thus mostly used in computational algorithms, where numerical methods and simulations involving numerical approximations of fractional derivatives are required. It is given by

$$ {}_{GL}D^{q}_{a,t} f(t) = \lim_{N\to\infty} h^{-q} \sum_{r=0}^{N-1} \frac{\Gamma(r-q)}{\Gamma(r-1)\Gamma(-q)} f(t-rh), \tag{9} $$

where q, $m-1 < q < m$ ($m \in \mathbb{N}$), denotes the fractional order, and $h = \frac{t-a}{N}$ is the discretization step in the time domain.

2.2.1 Multi-degree-of-freedom systems comprising fractional derivative elements

The equation governing the dynamics of an MDOF nonlinear structural system comprising fractional derivatives is given by [62]

$$ \mathbf{M}\ddot{\mathbf{x}} + \mathbf{C}\dot{\mathbf{x}} + \sum_{j=1}^{j_0} \mathbf{C}_j D^{q_j}(\mathbf{x}) + \mathbf{K}\mathbf{x} + \mathbf{h}(t, \mathbf{x}, \dot{\mathbf{x}}) = \mathbf{w}(t), \tag{10} $$

where $\mathbf{x} = \begin{bmatrix} x_0 & x_1 & \dots & x_{n-1} \end{bmatrix}^{\mathrm{T}}$ denotes the n-dimensional response displacement vector and a dot over a variable accounts for differentiation with respect to time. $\mathbf{M}$, $\mathbf{C}$, $\mathbf{C}_j$ and $\mathbf{K}$ denote the $n \times n$ mass, damping and stiffness matrices, and $\mathbf{h}(t, \mathbf{x}, \dot{\mathbf{x}})$ and $\mathbf{w}(t)$ denote the n-dimensional nonlinearity and system excitation vectors, respectively. The derivatives of fractional order q_j, $0 < q_j < 1$, are represented by the fractional operator $D^{q_j}(\cdot)$, which for the purposes of this paper is modeled by adopting the Caputo definition in Eq. (8) for $a = 0$ and $m = 1$, that is,

$$ D^{q_j}(x_i(t)) = \frac{1}{\Gamma(1-q_j)} \int_0^t \frac{\dot{x}_i(\tau)}{(t-\tau)^{q_j}}\, d\tau. \tag{11} $$

3 Efficient sampling methods for relaxed power spectral density estimation

In this section, the relaxed PSD concept, as well as various sampling methods that are used in the ensuing analysis are discussed.

3.1 Definition of the relaxed power spectral density function

The relaxed PSD function is a probabilistic representation of PSD functions ensemble, which share some similar characteristics, such as peak frequency and total power (e.g., [43, 44]). Its aim is to quantify uncertainties associated with the acquisition of real data records, as well as the PSD estimation process itself. To construct the relaxed PSD, an ensemble of N_e estimated PSD functions is considered. These functions are typically estimated from real or artificial time signals using a spectral estimation method, such as Welch's method. In this context, let s_{i,ω_n} denote the spectral value of the ith PSD estimate at frequency ω_n, where $i = 0, 1, \ldots, N_e - 1$, $\omega_n = n\Delta\omega$, and $n = 0, 1, \ldots, N_\omega - 1$, with N_ω representing the total number of frequency components. For each these component ω_n, the mean

$$\mu_{\omega_n} = \frac{1}{N_e} \sum_{i=0}^{N_e-1} s_{i,\omega_n} \tag{12}$$

and standard deviation

$$\sigma_{\omega_n} = \sqrt{\frac{1}{N_e} \sum_{i=0}^{N_e-1} \left(s_{i,\omega_n} - \mu_{\omega_n}\right)^2}, \tag{13}$$

are computed. These statistical moments characterize the variability of the ensemble at each frequency and form the basis of the relaxed PSD model.

A probability density function (PDF) is then defined for each frequency ω_n based on the corresponding μ_{ω_n} and σ_{ω_n} in Eqs. (12) and (13). To this end, a truncated normal distribution is often utilized, which has the form

$$f_{\omega_n}(s; \mu, \sigma, a, b) = \frac{1}{\sigma} \frac{\phi\left(\frac{s-\mu}{\sigma}\right)}{\Phi\left(\frac{b-\mu}{\sigma}\right) - \Phi\left(\frac{a-\mu}{\sigma}\right)}, \tag{14}$$

where $\phi(\eta) = \frac{1}{\sqrt{2\pi}} \exp\left(-\frac{1}{2}\eta^2\right)$ represents the standard normal distribution, and $\Phi(\zeta) = \frac{1}{2}\left(1 + \mathrm{erf}(\zeta/\sqrt{2})\right)$ is its corresponding cumulative distribution function (CDF), with $\mathrm{erf}(\cdot)$ denoting the error function. In Eq. (14), a and b correspond to the truncation bounds, while all subscripts are omitted for simplicity. As dependencies and correlations between frequencies are not considered in the original model, the probability density functions (PDF) has

to be determined separately for each individual frequency ω_n. Additionally, the lower truncation bound a is set equal to 0, as negative values are not physically meaningful for PSD functions. Therefore, the truncation bounds $a_{\omega_n} = 0$ and $b_{\omega_n} = \infty$ are considered in this paper. It should be noted that, depending on the data distribution, different probability density functions can be employed, providing flexibility in modeling uncertainties when deriving the relaxed PSD function. The interested reader is referred to [43] for a detailed discussion.

Following the adoption of a relaxed PSD function-based formulation, individual PSD functions can be sampled for further analysis, such as within a MCS framework. In essence, this approach enables the generation of random realizations that reflect the marginal statistical characteristics of the relaxed PSD. However, in the standard relaxed PSD model, as presented in Ref. [43], the sampling is performed independently at each frequency, meaning that the correlations between neighboring frequencies are not considered. Specifically, a separate probability density function is constructed for each frequency, and samples are drawn independently from these N_ω marginal distributions. While this method is computationally straightforward, it often leads to non-smooth or physically unrealistic PSD realizations that do not capture the coherent structure typically observed in empirical spectra. To address this limitation, the present work introduces enhanced sampling strategies that incorporate frequency-dependent correlations directly into the PSD generation process. By embedding cross-frequency dependencies into the sampling scheme, the proposed models yield smoother and more realistic PSD samples that better represent the underlying stochastic process. This not only improves the physical plausibility of the generated PSD functions but also enhances the accuracy of downstream reliability analyses, such as failure probability estimation under random excitation. The key novelty of this manuscript lies in the application of such correlation-aware PSD sampling models to dynamical systems that include fractional derivative elements. These systems are particularly sensitive to the spectral content of the input excitation due to their inherent memory and non-local behavior. Accurately capturing the frequency structure of the input process is therefore essential for meaningful reliability predictions. By combining correlated PSD sampling with fractional-order system dynamics, the proposed framework offers a more comprehensive and realistic approach to modeling uncertainty in complex engineering systems.

3.2 Sampling with one random variable

The first dependency sampling model, which is the simplest of those considered herein, is based on the use of a single random variable [45]. Specifically, first, a uniformly distributed variable $u \sim \mathcal{U}(0,1)$ is sampled, and then, the corresponding value X is obtained using the inverse CDF, that is $X = F^{-1}(u)$. It is noted that sampling from the inverse CDFs of the individual probability densities in the relaxed PSD function yields samples that are consistent with the respective target distributions. Clearly, the one-variable sampling model does not account for frequency correlations. Nevertheless, it is an efficient sampling method, not only because it requires a single random variable per PSD sample, i.e., $N_Z = 1$, but also because it can produce quite smooth realizations. However, it has limited flexibility as it may not fully capture variations or correlations in the data. In the ensuing analysis, this sampling approach is referred to as the one random variable (RV) model.

3.3 Sampling with multivariate Gaussian distributions

A more efficient approach has been proposed to bypass the limitations arising from the simplicity of the scheme involving sampling with one RV in Section 3.2. This pertains to modeling a multivariate Gaussian distribution based on the marginal PDFs of the relaxed PSD, while also accounting for correlations [45]. In this context, consider a random variable vector $\mathbf{X} = \begin{bmatrix} X_1 & X_2 & \dots & X_{N_\omega} \end{bmatrix}^{\mathrm{T}}$, with mean $\boldsymbol{\mu}_{\mathbf{X}}$ and covariance matrix $\boldsymbol{\Sigma}_{\mathbf{X}}$. The joint PDF is defined by

$$f(\boldsymbol{x}) = \frac{1}{\sqrt{(2\pi)^{N_\omega} \det(\boldsymbol{\Sigma}_{\mathbf{X}})}} \exp\left(-\frac{1}{2} (\boldsymbol{x} - \boldsymbol{\mu}_{\mathbf{X}})^{\mathrm{T}} \boldsymbol{\Sigma}_{\mathbf{X}}^{-1} (\boldsymbol{x} - \boldsymbol{\mu}_{\mathbf{X}}) \right). \tag{15}$$

A vector of independent standard Gaussian variables $\boldsymbol{z}$ is then defined as $\boldsymbol{x} = \boldsymbol{\mu} + \mathbf{L}\boldsymbol{z}$, ensuring the desired distribution and correlation structure. Here, $\mathbf{L}$ denotes the Cholesky factor of the covariance matrix $\boldsymbol{\Sigma}_{\mathbf{X}}$, fulfilling $\boldsymbol{\Sigma}_{\mathbf{X}} = \mathbf{L}\mathbf{L}^T$. This sampling model is efficient, numerically stable, and requires a relatively small amount of $N_{\mathrm{Z}} = N_\omega$ random variables. However, its accuracy depends on the presence of sufficient correlation in the data. While the method does not impose a theoretical limit on the dimensionality of the MVG distribution, its practical feasibility depends on the available computational resources and the structure of the covariance matrix. In the ensuing analysis, this approach is referred to as the multivariate Gaussian (MVG) model.

3.4 Sampling based on using the Ornstein-Uhlenbeck process

In this section, an approach for sampling PSD functions, considering also the correlations is presented. This sampling model is classified as Markov sampling, and is specifically designed to account for the relaxed PSD function $S(\omega)$ [45]. The resulting PSD function can be viewed as a sample trajectory of a non-stationary Ornstein-Uhlenbeck (OU) process with respect to frequency. By modeling the uncertainty in the relaxed PSD using observed data, the mean, the variance and the covariance of a PSD function $S(\omega)$ are given by

$$\mu_S(\omega) = \mathrm{E}[S(\omega)], \tag{16}$$

$$\sigma_S^2(\omega) = \mathrm{E}[S^2(\omega)] - \mathrm{E}^2[S(\omega)] \tag{17}$$

and

$$\sigma_S(\omega, \omega + \Delta\omega) = \mathrm{E}[S(\omega)S(\omega + \Delta\omega)] - \mathrm{E}[S(\omega)]\,\mathrm{E}[S(\omega + \Delta\omega)], \tag{18}$$

respectively. The statistical quantities defined in Eqs. (16) to (18) are deterministic functions with respect to ω and are calculated from the relaxed PSD at discrete points. Note, in passing, that the sampling model described by Eqs. (16) to (18) accounts only for modeling the dependencies between neighboring frequencies, improving in this way the sampling process.

As it is also mentioned above, the PSD function sampling follows a Markov process, where the first value S_1 is sampled from the PDF of the relaxed PSD. The subsequent values $S_2, S_3, \ldots, S_{N_\omega}$, are obtained by adding a term ΔS_j to account for correlations between neighboring frequencies. This process is described by

$$S_{j+1} = S_j + \Delta S_j, \tag{19}$$

where ΔS_j depends on a set of parameters λ_j and k_j, with $j = 1, 2, \ldots, n$ and reads

$$\Delta S_j = -k_j S_j + \lambda_j \Phi_j + \mu_{j+1} - (1 - k_j)\mu_j. \tag{20}$$

These parameters are determined by solving a system of linear equations which depend on variance and cross-correlation conditions, namely,

$$k_j = 1 - \frac{\sigma_{j,j+1}}{\sigma_j^2} \tag{21}$$

and

$$\lambda_j = \sqrt{\sigma_{j+1}^2 - \frac{\sigma_{j,j+1}}{\sigma_j^2}}, \tag{22}$$

for $j = 1, 2, \ldots, n$.

The structure of ΔS_j is inspired by a discretized Ornstein–Uhlenbeck process, which introduces damped stochastic perturbations to maintain continuity and correlation between neighboring frequency bins. However, unlike the classical Ornstein–Uhlenbeck model, the present formulation includes additional correction terms (involving μ_j and μ_{j+1}) to satisfy prescribed cross-correlation and variance constraints across the ensemble of PSD functions.

It is noted that following the sampling framework described by Eqs. (16) to (22), the resulting PSD functions are smooth, with strong correlations between adjacent frequencies. Subsequently, this provides a realistic representation of the data. Finally, the implementation of this sampling approach requires using $N_Z = N_\omega$ independent random variables, while it generates PSD functions that reflect efficiently the statistical properties of the observed data, in comparison to the sampling frameworks discussed in Sections 3.2 and 3.3. A detailed description of the sampling procedures described in Sections 3.2 to 3.4 can be found in Ref. [45].

4 Application of the proposed framework

4.1 Failure probability estimation for systems comprising fractional derivatives

The estimation of failure probability is crucial in stochastic dynamics, as it aims to assess the safety of structures and determine relevant safety margins [63, 64, 65, 66]. To conduct a precise probabilistic analysis for a system under consideration, the failure probability p_f is defined as

$$p_f = \int_{\mathcal{X}} I(x) f(x)\, dx, \tag{23}$$

where $f(x)$ denotes the PDF of the random variables and $I(x)$ is the indicator function defined as

$$I(x) = \begin{cases} 1, & \text{if } g(x) \leq 0 \\ 0, & \text{otherwise,} \end{cases} \tag{24}$$

with $g(x)$ as performance function, defining the failure region of the system. From a MCS perspective, as it is demonstrated in the present work, the failure probability can be defined as

$$p_f^{\mathrm{MC}} = \frac{1}{N_{MCS}} \sum_{i=1}^{N_{MCS}} I\left(x^{(i)}\right), \tag{25}$$

where N_{MCS} and $x^{(i)}$ denote the number of MCS samples and the ith system response, respectively.

In this context, considering Eq. (25), simulations are initially performed in the following using the individual estimated PSD functions of the ensemble (see Eqs. (5) and (6)) as the benchmark estimation, based on the raw and unprocessed data shown in Fig. 1. This is followed by simulations using the mean of the ensemble, and the uncorrelated relaxed PSD function model. Additionally, the three models described in Section 3, i.e., the one RV model, the MVG model and the correlated relaxed PSD model, are applied.

To ensure that the results obtained in the following numerical examples section are stable, a sufficiently large number of MCS samples is used. By doing so, it can be shown that the coefficient of variation (CoV) of the failure probability estimate, namely

$$\mathrm{CoV}(p_f) = \sqrt{\frac{1 - p_f}{p_f \cdot N_{MCS}}}, \tag{26}$$

is low enough. The latter indicates the stability of the results, and thus, that these can be considered reliable [29]. This is reported for the three dynamic models in the following analysis, in addition to the computed failure probabilities.

4.2 Spectral Representation Method

The spectral representation method (SRM) is one of the most widely used approaches to generate realizations of stationary and non-stationary stochastic processes, which are compatible with a given PSD function $S(\omega)$ [38, 67]; additional extensions of the SRM for reducing the involved random variables are found in [68, 69]. This method is particularly useful when the objective is to generate artificial signals in the time domain, whose statistical properties satisfy a predefined spectral description. For the stationary case, which is

also of interest in the present paper, the process realization is constructed using the following expression

$$f(t) = \sqrt{2} \sum_{n=0}^{N_\omega - 1} \left(2S(\omega_n)\Delta\omega\right)^{1/2} \cos(\omega_n t + \phi_n). \tag{27}$$

In Eq. (27), ω_n represents the discretized angular frequencies and $\Delta\omega = \omega_u/N_\omega$ is the frequency discretization step, with ω_u accounting for the upper cut-off frequency. Further, ϕ_n are random phase angles uniformly distributed over $[0, 2\pi]$, N_ω denotes the total number of frequency points used in the discretization, and t is the time variable at which the process is evaluated. Employing Eq. (27) to generate multiple realizations with different random phase sets $\{\phi_n\}$, a variety of process samples can be obtained, each statistically consistent with the original PSD $S(\omega)$.

4.3 Utilized PSD functions and sample derivation

For the numerical implementation, a set of predefined PSD functions is considered, and the SRM (see Eq. (27)) is used to generate 30 realizations of stochastic processes compatible with each of the PSDs. Noting that the random phase angles in the application of the SRM lead to different realizations, even when these are based on the same underlying PSD function, the constructed time signals are regarded as input data, emulating real data. Subsequently, an ensemble of PSD estimates is constructed. This is done by using Welch's method to transform the above time signals into the frequency domain (see Eqs. (5) and (6)). The ensemble of PSD estimates reflects the inherent uncertainties present in real data and serves as a representative dataset for the following analysis.

Welch's method is chosen particularly for its ability to produce smoother and more stable spectral estimates compared to non-averaging methods, such as the classical periodogram. This smoothing effect is crucial in the context of the proposed approach, as highly oscillatory PSD estimates, often produced by raw periodograms, can distort the underlying spectral structure and obscure statistical correlations across frequencies. The use of Welch's method thus supports the identification and modeling of frequency-dependent dependencies, which form the foundation for the correlation-aware sampling strategy presented in this work. However, it is important to note that the parameters of Welch's method, such as segment length, window function,

and degree of overlap, do influence the resulting PSD estimates. These parameters affect both spectral resolution and variance reduction, thereby influencing how well frequency correlations are preserved in the estimated dataset. In this work, the Welch parameters are selected carefully to strike a balance between smoothness and resolution, ensuring that the generated PSD ensemble remains both physically meaningful and statistically robust for subsequent reliability analysis.

The first PSD function that is utilized in the following is the Clough-Penzien PSD function is used to generate realizations for the following examples [70]. It is given by

$$S^{\mathrm{CP}}(\omega, S_0, \omega_f, \zeta_f, \omega_g, \zeta_g) = S_0 \cdot \frac{\omega_g^4 + 4\zeta_g^2\omega_g^2\omega^2}{(\omega_g^2 - \omega^2)^2 + 4\zeta_g^2\omega_g^2\omega^2} \cdot \frac{\omega^4}{(\omega_f^2 - \omega^2)^2 + 4\zeta_f^2\omega_f^2\omega^2}, \tag{28}$$

where ω_g and ζ_g are the natural frequency and damping ratio of the soil, respectively, ω_f and ζ_f are the corresponding parameters for the bedrock, and S_0 corresponds to the intensity of the input white noise excitation process. Eq. (28) extends the Kanai-Tajimi PSD model [71, 72] by incorporating the filtering effects of both the soil and underlying bedrock. It provides a more comprehensive representation of ground motion by considering the transmission of seismic waves through multiple layers. The first term on the right-hand side of Eq. (28) represents the soil's filtering effect, which is similar to the Kanai-Tajimi model, while the second term accounts for the filtering characteristics of the bedrock. This dual-filter approach enables a more accurate characterization of ground motion, especially in regions where both soil and bedrock properties significantly influence the seismic response. The Clough-Penzien model is particularly useful for advanced structural analyses where precise modeling of seismic excitation is required. In the following examples, realizations compatible with Eq. (28) are generated by considering the parameters: $\omega_g = 8\pi$ rad/s and $\zeta_g = 0.6$ for the soil, $\omega_f = 0.8\pi$ rad/s and $\zeta_f = 0.6$ for the bedrock [73], and $S_0 = 1 \cdot 10^{-4}$ for the intensity of the white noise process. Stochastic processes are generated using time signals with a length of $T = 10$ s, a $\Delta t = 0.0209$ s time increment, and a frequency discretization of $\Delta\omega = 1.1719$ rad/s, with cut-off frequency set to $\omega_u = 150$ rad/s.

The second PSD function utilized in this work is the Davenport wind PSD [74, 26], which is widely used to model wind-induced excitations on

structures. It is given by

$$S^{\mathrm{D}}(\omega, K, V_{10}, c_1) = 4KV_{10}^2 \cdot \frac{f_1^2}{\omega(1+f_1^2)^{4/3}} \tag{29}$$

with $f_1 = \frac{c_1\omega}{\pi V_{10}}$, where ω denotes the circular frequency, V_{10} is the mean wind speed at a reference height of 10 m, c_1 is a length parameter related to the observation height or aerodynamic roughness, and K is an empirical scaling constant that determines the overall energy level of the spectrum. The dimensionless quantity f_1 represents a normalized frequency that accounts for wind speed and vertical scale. Eq. (29) captures the decay of turbulence energy across frequencies and has been extensively validated against field measurements for atmospheric boundary layer flows. The spectrum exhibits a peak at a characteristic frequency and decays with a slope, reflecting the inertial subrange and dissipation scales of turbulence. Its simplicity and physical interpretability make it a common choice in wind engineering and stochastic dynamic analyses. In the following examples, realizations compatible with Eq. (29) are generated by using the parameters $V_{10} = 10$ m/s, $c_1 = 5$ m, and $K = 0.01$. Stochastic processes are generated using time signals with a duration of $T = 30$ s, a time increment of $\Delta t = 0.157$ s, and a frequency discretization of $\Delta\omega = 0.209$ rad/s, with cut-off frequency set to $\omega_u = 20$ rad/s.

The last PSD function employed in the following case studies section is the JONSWAP (Joint North Sea Wave Project) spectrum [75], which was originally developed to characterize the energy distribution of wind-generated sea waves. It is given by

$$S^{\mathrm{J}}(\omega, \alpha, \omega_p, \gamma) = \frac{\alpha g^2}{\omega^5} \exp\left(-\frac{5}{4}\left(\frac{\omega_p}{\omega}\right)^2\right) \gamma^{\exp\left(\frac{-(\omega-\omega_p)^2}{2\sigma^2\omega_p^2}\right)}, \tag{30}$$

where ω is the circular frequency, ω_p is the peak frequency, α is a scaling parameter related to the energy level, γ is the peak enhancement factor, and g is the gravity acceleration. The parameter σ controls the width of the peak and is defined piecewise as

$$\sigma = \begin{cases} \sigma_a, & \omega \leq \omega_p \\ \sigma_b, & \omega > \omega_p \end{cases}, \tag{31}$$

with σ_a and σ_b denoting parameters to be specified. Eq. (30) allows for the modeling of strongly peaked spectra and is well suited for applications

requiring realistic representations of stochastic broadband excitation with pronounced dominant frequencies. Although originally derived from oceanographic measurements, the JONSWAP spectrum has found application in structural reliability studies as a flexible and physically motivated alternative to classical models like the Clough-Penzien PSD model. For generating realizations compatible with Eq. (30), the following set of parameters are used: $\omega_p = 2$ rad/s, $\gamma = 3.3$, $\alpha = 0.005$, $\sigma_a = 0.7$, and $\sigma_b = 0.9$. A time signal of duration $T = 60$ s and increment $\Delta t = 0.2094$ s is used, with a frequency resolution of $\Delta\omega = 0.1047$ rad/s and an upper cut-off frequency $\omega_u = 15$ rad/s.

The datasets generated considering the PSD functions in Eqs. (28), (29), and (30), respectively, are shown in Fig. 1. Using these datasets, a relaxed PSD function is constructed for each case, and is subsequently used for uncertainty quantification. The constructed probabilistic PSD functions are shown in Fig. 2 for reference. A detailed description of the followed procedure can be found in Section 3 (see also [43]).

Subsequently, the relaxed PSD functions are utilized to estimate the failure probabilities for the systems, including a Duffing nonlinear oscillator, a TMDI system, and an vibration energy harvesting device, each equipped with fractional derivative elements. Indicative examples of PSD functions sampled with the schemes described in Sections 3.2 to 3.4 are shown in Fig. 3.

5 Numerical examples

In this section, three numerical examples including systems endowed with fractional derivative elements are used to demonstrate the validity and efficiency of the proposed framework. These are a Duffing nonlinear oscillator, a TMDI, and a vibration energy harvesting device.

5.1 Duffing nonlinear oscillator comprising fractional derivatives

The equation of motion of a Duffing nonlinear oscillator with fractional derivative elements is given by

$$m\ddot{x}(t) + cD^q x(t) + kx(t) + h(t,x) = F(t), \tag{32}$$

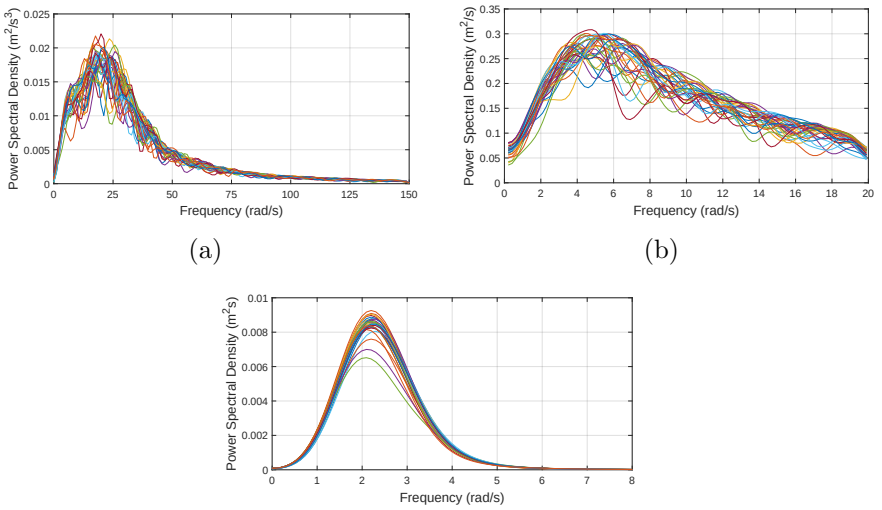

Figure 1: Datasets compatible with (a) the Clough-Penzien PSD function in Eq. (28), (b) the Davenport PSD function in Eq. (29), and (c) the JONSWAP PSD function in Eq. (30), estimated with Welch's method.

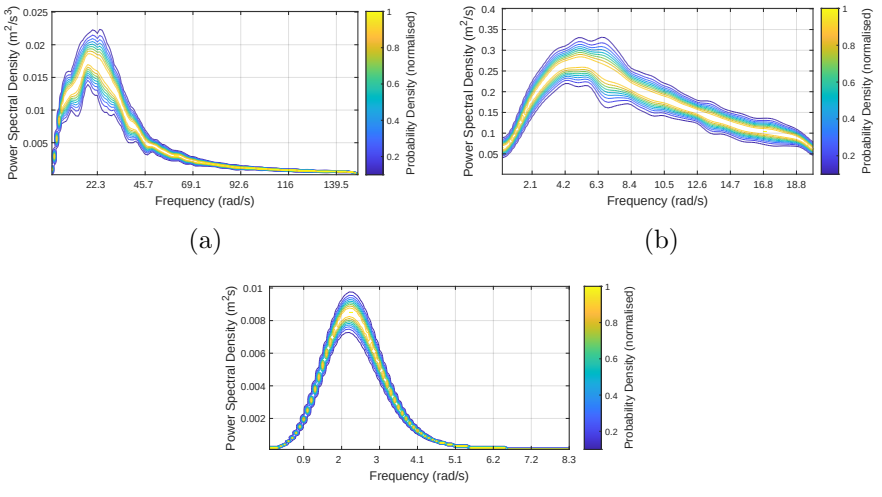

Figure 2: Relaxed PSD functions constructed by the three datasets in Fig. 1: (a) relaxed PSD of the Clough-Penzien dataset; (b) relaxed PSD of the Davenport dataset; (c) relaxed PSD of the JONSWAP dataset.

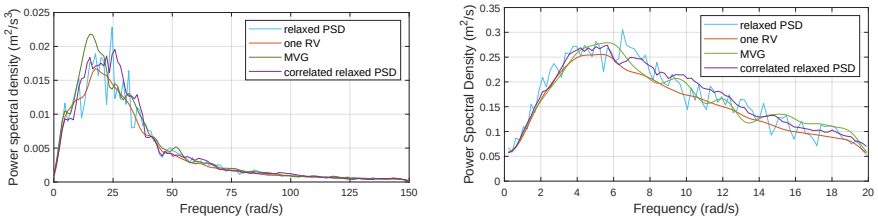

(a)

(b)

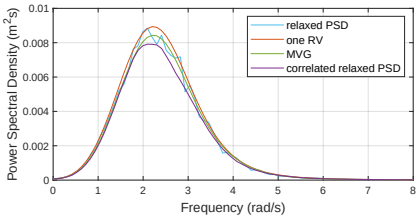

(c)

Figure 3: Generated PSD samples for the different sampling schemes in Sections 3.2 to 3.4 for the presented datasets: (a) PSD samples compatible with the Clough-Penzien PSD function in Eq. (28); (b) PSD samples compatible with the Davenport PSD function in Eq. (29); (c) PSD samples compatible with the JONSWAP PSD function in Eq. (30).

where m represents the mass of the system, and c and k denote the damping and stiffness coefficients, respectively. The function

$$h(t, x) = \varepsilon k x^3(t) \tag{33}$$

describes the nonlinearity of the system, with $\varepsilon > 0$ denoting a coefficient that controls its magnitude. Further, $D^q(\cdot)$, $0 < q < 1$, represents the fractional derivative operator defined as the Caputo fractional derivative of Eq. (11) with fractional order q. The term $F(t)$ is the external stochastic excitation such that $F(t) = -ma_g(t)$, where $a_g(t)$ is a ground motion acceleration described by the Clough-Penzien PSD form in Eq. (28). In this numerical example, the following structural parameters are used: $m = 0.5$, $c = 0.05$, $k = 150$, $q = 0.5$, and $\varepsilon = 1$.

Next, a performance function is defined to measure the deviation of the system in Eq. (32) from a pre-determined behavior. This is defined as

$$g(x) = x_{crit} - \max_{t \in T} |x| \,, \tag{34}$$

where x_{crit} represents a critical value, set in the following equal to $x_{crit} = 0.07$, and $\max_{t \in T} |x|$ represents the maximum displacement of the oscillator over the time interval T. Thus, any displacement larger than the critical value x_{crit} at any time instant within T is considered a system failure.

The SRM is employed to generate realizations of the excitation process $a_g(t)$ that conform to the PSD described by Eq. (28), also illustrated in Fig. 1a. A total of $N_{MCS} = 10^6$ samples are produced to achieve a reliable empirical estimate of the failure probability.

These simulations are based on an ensemble of N_e PSD functions, sampled from the underlying probabilistic model, each representing a possible realization of the spectral content of the excitation. For each PSD in this ensemble, corresponding time-domain samples are generated using the spectral representation method, allowing for the stochastic nature of the excitation and the variability across different PSD realizations to be taken into account. Each time signal is then applied to the dynamical system defined by Eqs. (32) and (33). The system response is computed using the L1 algorithm [76], which provides a numerical approximation of the Caputo fractional derivative in Eq. (32). Subsequently, the resulting responses are evaluated based on the failure criterion in Eq. (34). The benchmark failure probability is obtained by averaging over all N_{MCS} simulated responses, ensuring a robust and representative assessment of the failure probability that accounts for both the random excitation and variability in spectral content.

To ensure a consistent comparison, the same number of time series samples is used to evaluate the failure probability for both the benchmark and the correlations models. In all cases, a total of N_{MCS} individual PSD functions are sampled, either from the standard relaxed PSD model (benchmark) or from the correlated models. For each PSD realization, a single time series is generated using SRM and applied to the system, and the resulting system response is computed and checked against the failure criterion. This one-to-one sampling and simulation procedure ensures that all models are evaluated under identical conditions in terms of sample size, excitation variability, and numerical integration, with the only difference being the statistical structure of the underlying PSD model.

Further, the failure probability is calculated using the relaxed PSD methodology outlined in Section 3. The resulting failure probabilities for the individual models and sampling strategies are presented in Table 1. It can be seen that the MVG model closely matches the benchmark solution, whereas the models with one RV and the correlated relaxed PSD slightly overestimate the failure probability. Thus, it can be argued that they lead to a more conservative prediction. Conversely, the mean and relaxed PSD models underestimate the failure probability. The CoVs presented in Table 1 demonstrate the stability of the MCS-based estimate, indicating, in turn, low variability and consistency of the obtained results. In addition, the absolute percentage error (APE) is presented in Table 1. The APE is computed as

$$\mathrm{APE} = \left| \frac{p_{f,\mathrm{model}} - p_{f,\mathrm{benchmark}}}{p_{f,\mathrm{benchmark}}} \right| \cdot 100, \tag{35}$$

where $p_{f,\mathrm{model}}$ is the value obtained from a given model, and $p_{f,\mathrm{benchmark}}$ is the reference value used for comparison. The result is expressed as a percentage and quantifies the relative deviation of the model output from the benchmark solution.

5.2 Nonlinear tuned mass-damper-inerter system comprising fractional derivatives

In this section, a TMDI nonlinear system comprising a fractional derivative element is considered to verify the effectiveness of the proposed framework. Generally, TMDI systems are advancements of the traditional tuned mass-damper (TMD) concept used in passive vibration control, leveraging the

Table 1: Failure probabilities, absolute percentage error and CoV for the Duffing nonlinear oscillator with fractional derivative terms in Eqs. (32) and (33); comparison of different sampling schemes.

Model	$g(x)$	APE_g [%]	CoV
benchmark	0.0195	—	0.0071
mean	0.0147	24.62	0.0082
relaxed PSD	0.0158	18.97	0.0079
one RV	0.0250	28.21	0.0062
MVG	0.0196	0.51	0.0071
correlated relaxed PSD	0.0214	9.74	0.0068

mass amplification effect of the inerter–a two-terminal flywheel device that generates forces proportional to the relative acceleration between its terminals [77, 78, 62]. These systems have been widely utilized in engineering practice to mitigate unwanted vibrations in structures and mechanical systems. An indicative TMDI system that is used in the following analysis is shown in Fig. 4.

The governing equation of motion of the TMDI nonlinear system of primary mass m_1 and tuned mass m_2 is given by Eq. (10) for $j_0 = 1$. Assuming that the system response displacement is $\mathbf{x} = \begin{bmatrix} x_1 & x_2 \end{bmatrix}^{\mathrm{T}}$, the corresponding derivative of fractional order q_1 $(0 < q_1 < 1)$ is written as $D^{q_1}[\mathbf{x}] = \begin{bmatrix} \dot{x}_1 & D^{q_1} x_2 \end{bmatrix}^{\mathrm{T}}$. Therefore,

$$\mathbf{M} = \begin{bmatrix} m_1 & 0 \\ 0 & m_2 + b \end{bmatrix}, \ \mathbf{C} = \begin{bmatrix} c_1 + c_2 & 0 \\ -c_2 & 0 \end{bmatrix}, \ \mathbf{C}_1 = \begin{bmatrix} 0 & -c_2 \\ 0 & c_2 \end{bmatrix}, \ \mathbf{K} = \begin{bmatrix} k_1 + k_2 & -k_2 \\ -k_2 & k_2 \end{bmatrix} \tag{36}$$

denote the parameter matrices of the system, where c_1 and c_2 refer to the damping coefficients, and k_1 and k_2 are the stiffness coefficients. The parameter b is a mass-equivalent constant of proportionality. Furthermore, the system nonlinearity has the form

$$\mathbf{h}(t, \mathbf{x}, \dot{\mathbf{x}}) = \begin{bmatrix} \varepsilon k_1 x_1^3 \\ 0 \end{bmatrix} \tag{37}$$

with ε denoting the nonlinearity magnitude. $\mathbf{w}(t) = \begin{bmatrix} w(t) & 0 \end{bmatrix}^{\mathrm{T}}$ is the applied excitation, with $w(t)$ a stochastic process described by the Davenport PSD form in Eq. (29). An overview of the structural parameter values used for the TMDI system in Fig. 4 is given in Table 2.

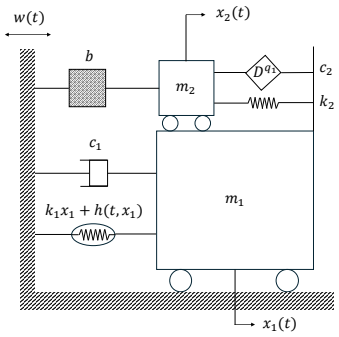

Figure 4: A TMDI nonlinear system with a fractional derivative element subjected to stochastic excitation.

Table 2: Parameter values for the TMDI nonlinear system in Eqs. (36) and (37).

Parameter	Variable	Value	Unit
Primary mass	m_1	11	kg
Tuned mass	m_2	1	kg
Mass-equivalent constant	b	1.1	kg
Damping coefficient of primary mass	c_1	1	Ns/m
Damping coefficient of tuned mass	c_2	0.78	Ns/m
Stiffness of primary mass	k_1	972	N/m
Stiffness of tuned mass	k_2	124	N/m
Fractional derivative order	q_1	0.5	[-]
Intensity of the nonlinearity	ε	0.1	[-]

The deviation of the system response from a pre-determined threshold is examined next by defining the performance function for the primary mass as

$$g_1(x_1) = x_{1,crit} - \max_{t\in T} |x_1| \,, \tag{38}$$

and the performance function for the tuned mass as

$$g_2(x_2) = x_{2,crit} - \max_{t\in T} |x_2| \,. \tag{39}$$

In Eqs. (38) and (39), $x_{1,crit}$ and $x_{2,crit}$ denote the critical values which characterize the maximum displacement boundaries of the system, and in the ensuing analysis are set equal to $x_{1,crit} = 2.5$ and $x_{2,crit} = 0.85$, respectively. Furthermore, $\max_{t\in T} |x_i|$ accounts for the maximum displacement of mass i ($i = 1, 2$) over the time interval T. Considering that the TMDI nonlinear system is a 2-DOF system, failure is assumed to occur if either of the performance conditions in Eqs. (38) and (39) is violated. Therefore, the combined performance function is expressed as

$$g(\mathbf{x}) = \min \{g_1(x_1), g_1(x_2)\} \,, \tag{40}$$

where $g(\mathbf{x}) < 0$ indicates system failure.

Next, the SRM is utilized to generate ground motion process realizations $w(t)$ consistent with the prescribed PSD in Eq. (28), also shown in Fig. **??**. A sufficiently high number of MCS samples is considered, i.e., $N_{MCS} = 10^5$, for accurate estimation of the empirical failure probability. For each input realization, the response is determined by solving the fractional differential equation defined by Eqs. (32) and (33) using the L1 algorithm [76]. The obtained responses are evaluated based on the performance functions in Eqs. (38) to (40) to identify failure cases, with the failure probability being estimated from the proportion of samples exceeding the defined limits; see also Eqs. (25) and (26).

Table 3 summarizes the failure probabilities for the TMDI nonlinear system for each of the three performance functions in Eqs. (38) to (40). Across all three criteria, the MVG model shows the closest agreement with the benchmark results, demonstrating its accuracy in estimating failure probabilities. The correlated relaxed PSD model also provides comparable results, although it yields slightly differing failure probabilities for the performance functions in Eqs. (38) to (40). The MVG model yields higher failure probabilities, indicating more conservative estimates. In contrast, the mean and

relaxed PSD model consistently underestimate failure probabilities across all criteria, indicating a lack of correlation structure. These observations highlight the influence of the chosen estimation model on the resulting failure probabilities and emphasize the importance of model selection for accurate reliability assessment. The corresponding CoVs are given in Table 4. They indicate that the results are stable and consistent.

Table 3: Failure probabilities for the TMDI nonlinear system with fractional derivatives in Eqs. (36) and (37); comparison of different sampling schemes.

Model	$g_1(x_1)$	APE_{g_1} [%]	$g_2(x_T)$	APE_{g_2} [%]	$g(\mathbf{x})$	APE_g [%]
benchmark	0.0046	—	0.0048	—	0.0083	—
mean	0.0026	44.04	0.0029	40.18	0.0062	25.15
relaxed PSD	0.0023	50.50	0.0027	44.31	0.0059	28.77
one RV	0.0066	42.09	0.0065	34.00	0.0117	41.29
MVG	0.0048	3.31	0.0052	7.26	0.0087	5.03
correlated relaxed PSD	0.0042	9.60	0.0052	7.26	0.0089	7.45

Table 4: CoV for the TMDI nonlinear system with fractional derivatives in Eqs. (36) and (37); comparison of different sampling schemes.

Model	$g_1(x_1)$	$g_2(x_2)$	$g(\mathbf{x})$
benchmark	0.0463	0.0453	0.0346
mean	0.0619	0.0586	0.0400
relaxed PSD	0.0659	0.0608	0.0410
one RV	0.0388	0.0391	0.0291
MVG	0.0455	0.0437	0.0338
correlated relaxed PSD	0.0487	0.0437	0.0334

5.3 Nonlinear vibration energy harvesting system comprising fractional derivatives

The last numerical simulation in this paper pertains to a nonlinear vibration energy harvesting device with fractional derivative elements in the mechanical component (e.g., [6, 62]). One of the most commonly researched electromechanical energy harvesting devices is a system consisting of a cantilever beam equipped with piezoelectric patches positioned near its fixed ends; see Fig. 5.

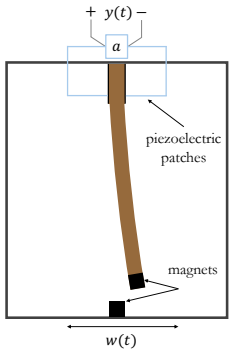

Figure 5: A nonlinear vibration energy harvesting system with a fractional derivative element subjected to stochastic excitation.

The dynamic and the electric behavior of such a system are represented by a set of coupled electromechanical equations, whose non-dimensional form is written in the form of Eq. (10) for $j_0 = 1$.

Next, assume that the system response displacement is denoted by $\mathbf{x} = \begin{bmatrix} x & y \end{bmatrix}^{\mathrm{T}}$, with x and y representing the displacement of the mechanical component and the induced voltage in the electrical component, respectively. Then, the derivative of fractional order q_1 $(0 < q_1 < 1)$ becomes $D^{q_1}[\mathbf{x}] = \begin{bmatrix} D^{q_1}x & 0 \end{bmatrix}^{\mathrm{T}}$. The parameter matrices of the system are given by [62]

$$\mathbf{M} = \begin{bmatrix} 1 & 0 \\ 0 & 0 \end{bmatrix}, \ \mathbf{C} = \begin{bmatrix} 2\zeta & 0 \\ -1 & 0 \end{bmatrix}, \ \mathbf{C_1} = \begin{bmatrix} 0 & 0 \\ 0 & 1 \end{bmatrix}, \ \mathbf{K} = \begin{bmatrix} 1 & \kappa^2 \\ 0 & \alpha \end{bmatrix}, \tag{41}$$

while the nonlinear vector of the system is

$$\mathbf{h}(t, \mathbf{x}, \dot{\mathbf{x}}) = \begin{bmatrix} \delta x^2 + \beta x^3 \\ 0 \end{bmatrix}. \tag{42}$$

The excitation vector is $\mathbf{w} = \begin{bmatrix} w(t) & 0 \end{bmatrix}^{\mathrm{T}}$, where $w(t)$ is a stochastic process described by the JONSWAP PSD form in Eq. (30). The set of parameter values used for the nonlinear harvesting device are included in Table 5.

Next, a set of performance functions is defined to examine the response behavior of the system. Specifically, the performance function for the mechanical component is defined as

$$g_x(x) = x_{crit} - \max_{t \in T} |x| \,, \tag{43}$$

Table 5: Parameter values for the nonlinear vibration energy harvesting system in Eqs. (41) and (42).

Variable	ζ	κ	α	δ	β	q_1
Value	0.15	0.5	0.05	0.2	0.05	0.5

while the corresponding function for the electrical component is defined as

$$g_y(y) = y_{crit} - \max_{t \in T} |y| \,, \tag{44}$$

with $x_{crit} = 0.7$ and $y_{crit} = 0.346$ denoting the critical values that characterize the maximum displacement boundaries of the system. Further, $\max_{t \in T} |v|$ represents the maximum value that the variable v, with $v \in \{x, y\}$, may attain over the time interval T. Considering that failure occurs based on violation of the either performance functions in Eqs. (43) or (44), the combined performance function for this case is defined as

$$g(\mathbf{x}) = \min \{g_x(x), g_y(y)\} \,. \tag{45}$$

Then, the failure probability is calculated by generating samples using the SRM. Each sample is applied to the system, and the corresponding system response is evaluated. Failure is determined by whether the response exceeds a predefined threshold, as this is specified by Eqs. (43) to (45). Specifically, a total of $N_{MCS} = 10^5$ MCS samples are generated, and the L1 algorithm [76] is used to solve the fractional differential equation defined by Eqs. (32) and (33), and compute the corresponding responses. Similar to the examples in Sections 5.1 and 5.2, the total number of samples is such that the obtained results lead to a statistically reliable analysis of the system's behavior.

The failure probabilities for the nonlinear vibration energy harvesting system are shown in Table 6. Their calculation has been done by employing the performance functions in Eqs. (43) to (45). Clearly, the results obtained by the correlated relaxed PSD model and the MVG model are closely aligned with the benchmark across all criteria, indicating a high accuracy level. On the other hand, the one RV model tends to overestimate the failure probabilities, resulting in slightly more conservative predictions. In contrast, the mean and the relaxed PSD models produce lower estimates, underestimating the failure probabilities. These results highlight the variability in prediction accuracy depending on the chosen estimation approach and underscore the importance of model selection for reliable failure probability assessment. Finally, the CoVs presented in Table 7 show stable results with low variance.

Table 6: Failure probabilities for the nonlinear vibration energy harvesting system in Eqs. (41) and (42); comparison of different sampling schemes.

Model	$g_x(x)$	APE_{g_x} [%]	$g_y(y)$	APE_{g_y} [%]	$g(\mathbf{x})$	APE_g [%]
benchmark	0.0024	—	0.0024	—	0.0026	—
mean	0.0019	19.14	0.0018	23.47	0.0020	23.24
relaxed PSD	0.0019	18.26	0.0020	15.38	0.0021	18.50
one RV	0.0029	21.97	0.0029	22.45	0.0031	20.25
MVG	0.0024	0.34	0.0024	1.19	0.0025	1.68
correlated relaxed PSD	0.0025	3.72	0.0024	1.61	0.0026	3.02

Table 7: CoV for the nonlinear vibration energy harvesting system in Eqs. (41) and (42); comparison of different sampling schemes.

Model	$g_x(x)$	$g_y(y)$	$g(\mathbf{x})$
benchmark	0.0650	0.0652	0.0625
mean	0.0723	0.0745	0.0714
relaxed PSD	0.0719	0.0708	0.0693
one RV	0.0588	0.0588	0.0570
MVG	0.0649	0.0647	0.0630
correlated relaxed PSD	0.0638	0.0646	0.0616

6 Concluding remarks

In this paper, a relaxed PSD framework was presented and evaluated for quantifying uncertainties in dynamical systems that involve fractional derivative elements. The incorporation of fractional calculus enables more realistic modeling of complex material behaviors and memory effects, which are particularly relevant under stochastic excitation. To demonstrate the effectiveness of the proposed framework, three representative systems were analyzed: a Duffing nonlinear oscillator, a tuned mass-damper-inerter nonlinear system, and a nonlinear vibration energy harvester. These case studies highlighted the importance of accounting for frequency-domain correlation structures when estimating failure probabilities. The results indicated that probabilistic models incorporating such structures, especially the multivariate Gaussian and correlated relaxed PSD approaches, yield significantly improved accuracy and reliability in failure assessment. By capturing frequency dependencies, these models reduce the risk of underestimating system failure, ultimately

leading to more robust and conservative design strategies. Nevertheless, the proposed approach present certain challenges. First, its computational cost increases with the number of frequency components, particularly due to the need to store and manipulate high-dimensional covariance matrices. Additionally, the accuracy of the correlation structure depends on the availability and quality of spectral information, which may be limited in real-world applications. Finally, while the relaxed PSD formulation introduces flexibility, it may require careful calibration to avoid overly conservative or non-physical results. Future research should address these challenges by developing efficient approximation techniques for large-scale problems, incorporating data-driven or physics-informed priors for correlation modeling, and validating the framework across a broader class of dynamical systems. Furthermore, integrating the relaxed PSD methodology into practical engineering workflows remains an essential step to maximize its impact on reliability-based design and analysis.

CRediT authorship contribution statement

M. Behrendt: Formal analysis, Visualization, Funding acquisition, Methodology, Software, Writing – original draft. **V.C. Fragkoulis:** Conceptualization, Methodology, Software, Writing – review and editing. **G.D. Pasparakis:** Methodology, Visualization, Software, Writing – review and editing. **M. Beer:** Project administration, Funding acquisition, Supervision.

Declaration of competing interest

The authors declare that they have no known competing financial interests or personal relationships that could have appeared to influence the work reported in this paper.

Data availability

No data was used for the research described in the article.

Acknowledgment

Marco Behrendt gratefully acknowledges the financial support by the Alexander von Humboldt Foundation. Michael Beer gratefully acknowledges the support by the German Research Foundation (Grant No. FR 4442/2-1).

References

[1] T. T. Soong, M. Grigoriu, Random Vibration of Mechanical and Structural Systems, Prentice-Hall, 1993.

[2] J. B. Roberts, P. D. Spanos, Random vibration and statistical linearization, Courier Corporation, 2003.

[3] A. K. Chopra, Dynamics of Structures: Theory and Applications to Earthquake Engineering, Prentice-Hall, 1995.

[4] M. Grigoriu, Stochastic Calculus, Birkhäuser Boston, Boston, MA, 2002.

[5] M. Di Paola, M. Zingales, Long-range cohesive interactions of non-local continuum faced by fractional calculus, International Journal of Solids and Structures 45 (21) (2008) 5642–5659.

[6] I. Petromichelakis, A. F. Psaros, I. A. Kougioumtzoglou, Stochastic Response Analysis and Reliability-Based Design Optimization of Nonlinear Electromechanical Energy Harvesters With Fractional Derivative Elements, ASCE-ASME J Risk and Uncert in Engrg Sys Part B Mech Engrg 7 (1) (2021) 010901.

[7] K. R. dos Santos, J. G. Duarte, Stochastic response determination of hysteretic vibratory energy harvesters with fractional derivatives via stochastic averaging, Journal of Engineering Mechanics 150 (7) (2024) 04024035.

[8] M. Di Paola, A. Pirrotta, A. Valenza, Visco-elastic behavior through fractional calculus: an easier method for best fitting experimental results, Mechanics of materials 43 (12) (2011) 799–806.

[9] A. Sofi, G. Muscolino, M. D. Paola, Reliability analysis of structures controlled by external fractional viscoelastic dampers with interval parameters, Acta Mechanica Sinica 39 (4) (2023) 722486.

[10] A. Sofi, G. Muscolino, Reliability sensitivity analysis of frame structures controlled by external fractional viscoelastic dampers, Probabilistic Engineering Mechanics (2025) 103740.

[11] I. A. Kougioumtzoglou, P. Ni, I. P. Mitseas, V. C. Fragkoulis, M. Beer, An approximate stochastic dynamics approach for design spectrum based response analysis of nonlinear structural systems with fractional derivative elements, International Journal of Non-Linear Mechanics 146 (2022) 104178.

[12] I. P. Mitseas, P. Ni, V. C. Fragkoulis, M. Beer, Survival probability surfaces of hysteretic fractional order structures exposed to non-stationary code-compliant stochastic seismic excitation, Engineering Structures 318 (2024) 118755.

[13] P. Ni, I. P. Mitseas, V. C. Fragkoulis, M. Beer, Spectral incremental dynamic methodology for nonlinear structural systems endowed with fractional derivative elements subjected to fully non-stationary stochastic excitation, Structural Safety 111 (2024) 102525.

[14] P. D. Spanos, G. I. Evangelatos, Response of a non-linear system with restoring forces governed by fractional derivatives—time domain simulation and statistical linearization solution, Soil Dynamics and Earthquake Engineering 30 (9) (2010) 811–821.

[15] B. Pomaro, P. D. Spanos, Extended statistical linearization approach for estimating non-stationary response statistics of systems comprising fractional derivative elements, Probabilistic Engineering Mechanics 74 (2023) 103471.

[16] Y. Luo, P. D. Spanos, Non-stationary response determination of linear systems/structures with fractional derivative elements, Reliability Engineering & System Safety 261 (2025) 111056.

[17] J. Xian, C. Su, Nonstationary random vibration analysis of fractionally-damped nonlinear systems by equivalent linearization based on explicit time-domain method, Reliability Engineering & System Safety (2025) 111452.

[18] M. Di Paola, G. Failla, A. Pirrotta, Stationary and non-stationary stochastic response of linear fractional viscoelastic systems, Probabilistic Engineering Mechanics 28 (2012) 85–90.

[19] Y. Zhang, S. Li, Z. Zhu, V. C. Fragkoulis, Approximate response determination of nonlinear oscillators with fractional derivative elements subjected to combined periodic and evolutionary stochastic excitations, Mechanical Systems and Signal Processing 229 (2025) 112485.

[20] Y. Luo, M.-Z. Lyu, J.-B. Chen, P. D. Spanos, Equation governing the probability density evolution of multi-dimensional linear fractional differential systems subject to gaussian white noise, Theoretical and Applied Mechanics Letters 13 (3) (2023) 100436.

[21] I. A. Kougioumtzoglou, A. F. Psaros, P. D. Spanos, Path Integrals in Stochastic Engineering Dynamics, Springer, 2024.

[22] A. Pirrotta, I. Kougioumtzoglou, A. Di Matteo, V. Fragkoulis, A. Pantelous, C. Adam, Deterministic and random vibration of linear systems with singular parameter matrices and fractional derivative terms, Journal of engineering mechanics 147 (6) (2021) 04021031.

[23] G. Pasparakis, V. Fragkoulis, Harmonic wavelets based response evolutionary power spectrum determination of linear and nonlinear structural systems with singular matrices, Mechanical Systems and Signal Processing 149 (2021) 107203.

[24] G. Pasparakis, I. Kougioumtzoglou, V. Fragkoulis, F. Kong, M. Beer, Excitation–response relationships for linear structural systems with singular parameter matrices: A periodized harmonic wavelet perspective, Mechanical Systems and Signal Processing 169 (2022) 108701.

[25] Y.-K. Lin, G.-Q. Cai, Probabilistic Structural Dynamics: Advanced Theory and Applications, McGraw-Hill New York, 1995.

[26] J. Li, J. Chen, Stochastic Dynamics of Structures, John Wiley & Sons, 2009.

[27] Y. Jiang, X. Zhang, M. Beer, M. G. Faes, C. Papadimitriou, H. Zhou, First excursion probability of dynamical systems: A review on computational methods, Mechanical Systems and Signal Processing 232 (2025) 112751.

[28] M. Barbato, J. P. Conte, Structural reliability applications of nonstationary spectral characteristics, Journal of engineering mechanics 137 (5) (2011) 371–382.

[29] E. Zio, The Monte Carlo Simulation Method for System Reliability and Risk Analysis, Springer Series in Reliability Engineering, Springer London, London, 2013.

[30] B. Ellingwood, M. Maes, F. Michael Bartlett, A. T. Beck, C. Caprani, A. Der Kiureghian, L. Dueñas-Osorio, N. Galvão, R. Gilbert, J. Li, J. Matos, Y. Mori, I. Papaioannou, R. Parades, D. Straub, B. Sudret, Development of methods of structural reliability, Structural Safety 113 (2025) 102474.

[31] G. Stefanou, The stochastic finite element method: Past, present and future, Computer Methods in Applied Mechanics and Engineering 198 (9) (2009) 1031–1051.

[32] K.-V. Yuen, Bayesian Methods for Structural Dynamics and Civil Engineering, John Wiley & Sons, 2010.

[33] H. A. Jensen, Design and sensitivity analysis of dynamical systems subjected to stochastic loading, Computers & Structures 83 (14) (2005) 1062–1075.

[34] P. D. Spanos, I. A. Kougioumtzoglou, Survival probability determination of nonlinear oscillators subject to evolutionary stochastic excitation, Journal of Applied Mechanics 81 (5) (2014) 051016.

[35] C. Dang, M. Beer, Semi-Bayesian active learning quadrature for estimating extremely low failure probabilities, Reliability Engineering & System Safety 246 (2024) 110052.

[36] C. Dang, M. A. Valdebenito, P. Wei, J. Song, M. Beer, Bayesian active learning line sampling with log-normal process for rare-event probability estimation, Reliability Engineering & System Safety 246 (2024) 110053.

[37] R. A. Muller, G. J. MacDonald, Ice ages and astronomical causes: data, spectral analysis and mechanisms, Springer Science & Business Media, 2002.

[38] M. Shinozuka, G. Deodatis, Simulation of stochastic processes by spectral representation, Applied Mechanics Reviews 44 (4) (1991) 191–204.

[39] P. D. Spanos, A. Di Matteo, H. Zhang, Q. Yue, Z. Xu, Estimation of evolutionary power spectra of univariate stochastic processes by energy-based reckoning, Reliability Engineering & System Safety 245 (2024) 109962.

[40] Y. Wu, J. Wang, J. Cheng, S. Yang, Dimension-reduction spectral representation of soil spatial variability and its application in the efficient reliability analysis of seismic response in tunnels, Reliability Engineering & System Safety 248 (2024) 110175.

[41] G. Deodatis, M. Shields, The spectral representation method: A framework for simulation of stochastic processes, fields, and waves, Reliability Engineering & System Safety 254 (2025) 110522.

[42] G. Muscolino, F. Genovese, A. Sofi, Reliability Bounds for Structural Systems Subjected to a Set of Recorded Accelerograms Leading to Imprecise Seismic Power Spectrum, ASCE-ASME Journal of Risk and Uncertainty in Engineering Systems, Part A: Civil Engineering 8 (2) (2022) 04022009.

[43] M. Behrendt, M. Bittner, L. Comerford, M. Beer, J. Chen, Relaxed power spectrum estimation from multiple data records utilising subjective probabilities, Mechanical Systems and Signal Processing 165 (2022) 108346.

[44] M. Bittner, M. Behrendt, M. Beer, Relaxed evolutionary power spectral density functions: A probabilistic approach to model uncertainties of non-stationary stochastic signals, Mechanical Systems and Signal Processing 211 (2024) 111210.

[45] M. Behrendt, M.-Z. Lyu, Y. Luo, J.-B. Chen, M. Beer, Failure probability estimation of dynamic systems employing relaxed power spectral density functions with dependent frequency modeling and sampling, Probabilistic Engineering Mechanics 75 (2024) 103592.

[46] Y. Guan, W. Li, D. Kozak, J. Zhao, Response and reliability analysis of a nonlinear VEH systems with FOPID controller by improved stochas-

tic averaging method and LBFNN algorithm, Reliability Engineering & System Safety 249 (2024) 110206.

[47] M.-Z. Lyu, Y.-Y. Liu, J.-B. Chen, A novel model and simulation method for multivariate Gaussian fields involving nonlinear probabilistic dependencies and different variable-wise spatial variabilities, Reliability Engineering & System Safety 260 (2025) 110963.

[48] R. H. Shumway, D. S. Stoffer, D. S. Stoffer, Time series analysis and its applications, Vol. 3, Springer, 2000.

[49] M. S. Bartlett, Smoothing periodograms from time-series with continuous spectra, Nature 161 (4096) (1948) 686–687.

[50] M. S. Bartlett, Periodogram analysis and continuous spectra, Biometrika 37 (1-2) (1950) 1–16.

[51] P. Welch, The use of fast Fourier transform for the estimation of power spectra: A method based on time averaging over short, modified periodograms, IEEE Transactions on Audio and Electroacoustics 15 (2) (1967) 70–73.

[52] R. W. Hamming, Digital filters, 3rd Edition, Dover civil and mechanical engineering, Dover Publications, 1997.

[53] J. Sabatier, O. P. Agrawal, J. A. Tenreiro Machado (Eds.), Advances in Fractional Calculus: Theoretical Developments and Applications in Physics and Engineering, Springer, Dordrecht, 2007.

[54] A. A. Kilbas, H. M. Srivastava, J. J. Trujillo, Theory and applications of fractional differential equations, Vol. 204, elsevier, 2006.

[55] A. Carpinteri, F. Mainardi, Fractals and fractional calculus in continuum mechanics, Vol. 378, Springer, 2014.

[56] K. Biswas, G. Bohannan, R. Caponetto, A. Mendes Lopes, J. A. Tenreiro Machado, Fractional-Order Devices, SpringerBriefs in Applied Sciences and Technology, Springer International Publishing, Cham, 2017.

[57] F. Mainardi, Fractional calculus and waves in linear viscoelasticity: an introduction to mathematical models, World Scientific, 2022.

[58] N. Makris, M. Constantinou, Spring-viscous damper systems for combined seismic and vibration isolation, Earthquake engineering & structural dynamics 21 (8) (1992) 649–664.

[59] I. Podlubny, Fractional differential equations: an introduction to fractional derivatives, fractional differential equations, to methods of their solution and some of their applications, Vol. 198, Elsevier, 1998.

[60] R. Hilfer, Applications of fractional calculus in physics, World scientific, 2000.

[61] K. Diethelm, The analysis of fractional differential equations: An application-oriented exposition using operators of caputo type, Lecture Notes in Mathematics (2004).

[62] G. D. Pasparakis, V. C. Fragkoulis, I. A. Kougioumtzoglou, On the efficacy of sparse representation approaches for determining nonlinear structural system equations of motion, ASCE-ASME J Risk and Uncert in Engrg Sys Part B Mech Engrg 11 (3) (2025).

[63] A. Di Matteo, P. Spanos, A. Pirrotta, Approximate survival probability determination of hysteretic systems with fractional derivative elements, Probabilistic Engineering Mechanics 54 (2018) 138–146.

[64] V. C. Fragkoulis, I. A. Kougioumtzoglou, Survival probability determination of nonlinear oscillators with fractional derivative elements under evolutionary stochastic excitation, Probabilistic Engineering Mechanics 71 (2023) 103411.

[65] D. Jerez, V. Fragkoulis, P. Ni, I. Mitseas, M. A. Valdebenito, M. G. Faes, M. Beer, Operator norm-based determination of failure probability of nonlinear oscillators with fractional derivative elements subject to imprecise stationary gaussian loads, Mechanical Systems and Signal Processing 208 (2024) 111043.

[66] P. Ni, D. J. Jerez, V. C. Fragkoulis, M. G. R. Faes, M. A. Valdebenito, M. Beer, Operator Norm-Based Statistical Linearization to Bound the First Excursion Probability of Nonlinear Structures Subjected to Imprecise Stochastic Loading, ASCE-ASME Journal of Risk and Uncertainty in Engineering Systems, Part A: Civil Engineering 8 (1) (2022) 04021086.

[67] J. Liang, S. R. Chaudhuri, M. Shinozuka, Simulation of nonstationary stochastic processes by spectral representation, Journal of Engineering Mechanics 133 (6) (2007) 616–627.

[68] J. Chen, W. Sun, J. Li, J. Xu, Stochastic Harmonic Function Representation of Stochastic Processes, Journal of Applied Mechanics 80 (1) (2013) 011001.

[69] J. Chen, L. Comerford, Y. Peng, M. Beer, J. Li, Reduction of random variables in the stochastic harmonic function representation via spectrum-relative dependent random frequencies, Mechanical Systems and Signal Processing 141 (2020) 106718.

[70] R. W. Clough, J. Penzien, Dynamics of Structures, 2nd Edition, McGraw-Hill, New York, 1993.

[71] K. Kanai, Semi-empirical formula for the seismic characteristics of the ground, Bulletin of the Earthquake Research Institute 35 (1957) 309–325.

[72] H. Tajimi, A statistical method of determining the maximum response of a building structure during an earthquake, in: Proceedings of the 2nd world conference of earthquake engineering, Vol. 11, 1960, pp. 781–797.

[73] G. Deodatis, Non-stationary stochastic vector processes: seismic ground motion applications, Probabilistic Engineering Mechanics 11 (3) (1996) 149–167.

[74] A. G. Davenport, The spectrum of horizontal gustiness near the ground in high winds, Quarterly Journal of the Royal Meteorological Society 87 (372) (1961) 194–211.

[75] K. F. Hasselmann, T. P. Barnett, E. Bouws, H. Carlson, D. E. Cartwright, K. Eake, J. Euring, A. Gicnapp, D. Hasselmann, P. Kruseman, et al., Measurements of wind-wave growth and swell decay during the Joint North Sea Wave Project (JONSWAP), Ergaenzungsheft zur Deutschen Hydrographischen Zeitschrift, Reihe A (1973).

[76] C. G. Koh, J. M. Kelly, Application of fractional derivatives to seismic analysis of base-isolated models, Earthquake engineering & structural dynamics 19 (2) (1990) 229–241.

[77] L. Marian, A. Giaralis, Optimal design of a novel tuned mass-damper-inerter (TMDI) passive vibration control configuration for stochastically support-excited structural systems, Probabilistic Engineering Mechanics 38 (2014) 156–164.

[78] I. G. Mavromatis, I. A. Kougioumtzoglou, A Reduced-Order Wiener Path Integral Formalism for Determining the Stochastic Response of Nonlinear Systems With Fractional Derivative Elements, ASCE-ASME J Risk and Uncert in Engrg Sys Part B Mech Engrg 9 (3) (2023) 031201.